Ballistic recovery in III-V nanowire transistors

M. J. Gilbert[a] and S. K. Banerjee
Microelectronics Research Center, University of Texas at Austin, Austin, Texas 78758

(Received 10 March 2006; accepted 21 November 2006; published 23 January 2007)

In recent years, a great deal of attention has been focused on the development of quantum wire transistors as a means of extending Moore's law. Here the authors present results of fully three-dimensional, self-consistent quantum mechanical device simulations of InAs trigate nanowire transistor. The effects of inelastic scattering have been included as real-space self-energy terms. They find that the position of dopant atoms in these devices can lead to a reduction in the amount of scattering the carriers experience. They find that the combination of deeply buried dopant atoms and the high energy localization of polar optical phonon processes allow devices to recover their ballistic behavior even in the presence of strong inelastic phonon processes. © *2007 American Vacuum Society.* [DOI: 10.1116/1.2409987]

I. INTRODUCTION

It has been a well established fact that the semiconductor industry must devise an alternative solution to the bulk silicon metal-oxide-semiconductor field-effect transistor (MOSFET) in order to continue the relentless scaling of device density. One of the most promising of these new technologies is the quantum wire MOSFET. Trigate devices offer greatly improved electrostatic control over the channel of the device when compared to the traditional MOSFET due to the presence of the additional gates.[1] With a device of this nature, it is necessary to use a simulation tool that takes into account the quantum confinement in the system. Previously, one only had confinement in the direction perpendicular to the gate, but the width of the channel is now on the order of the Fermi wavelength of the electron. There have been many different simulations of ballistic operation of these devices.[2,3] However, recent work has shown that there is limited applicability to the assumption that at channel lengths of ~ 10 nm the nature of the transport is ballistic.[4] Therefore, while examination of the ballistic limit may provide an interesting base line, we must include the role of scattering.

Within the last few years, there has been a renewed interest in the use of III-V materials instead of silicon for future generation transistors. Previous studies have shown that care must be taken in the fabrication of these devices or large increases in the output drain current (kink effect) occur.[5,6] Through the use of quantum wires with discrete subbands for the active regions of the device, the kink effect may be eliminated. Nevertheless, there has been interest in MOSFETs in these III-V materials for use in high speed logic applications.[7] Furthermore, owing to the increased mobilities offered by III-V materials, the possibility exists that devices that are shorter than the phonon scattering length can be fabricated. Typically when electrons interact with phonons they lose their phase information. During this process, the electrons also lose a portion of their energy. Therefore, if electron transit times are longer than the corresponding energy relaxation times, then ballistic behavior will prevail even in the presence of the electron-phonon interactions.[8]

In this article, we present the results of a three-dimensional, self-consistent, quantum mechanical device simulation of several trigate InAs quantum wire MOSFETs. Here we present results of 10 nm channel length devices both in the elastic limit, where we only include interactions with the dopant ions and with both elastic and inelastic effects [the effects of impurity, acoustic deformation potential, intervalley ($\Gamma \rightarrow X$ and $\Gamma \rightarrow L$), and polar optical phonon (POP) scattering as separable real-space self-energy terms]. We show that the inclusion of inelastic phonon processes does not have a significant effect on the InAs devices. This is due to the fact that the POP process becomes highly localized in space as the carriers gain energy leading to reduced scattering rates, thereby allowing the devices to regain ballistic characteristics.

II. DEVICE STRUCTURE AND METHOD

In Fig. 1, we display a top view schematic of the device geometry for an InAs MOSFET with a 9.69 nm long and 8.48 nm wide channel taken to lie in the x-y plane (the z axis is normal to the plane shown). The exact device dimensions (multiples of the lattice constant) have been included in this simulation to aid in the inclusion of the discrete dopants. The thickness of the InAs layer is 9.09 nm. The source and drain of the device are n type with a doping density of 6×10^{18} cm^{-3}, while the channel of the device is considered to be p type, but undoped. The gate material is assumed to be platinum and the gate oxide on each side is composed of 1 nm of hafnium oxide (HfO_2). Underneath the device, we have assumed a generic insulating substrate. The structure of the device with the 9.69 nm channel is exactly the same with the exception, of course, of the channel length. Once the device geometry is defined, the InAs lattice is scanned, and the dopants are distributed according to the method presented in Ref. 9. Following the distribution of the dopants, they are then mapped back onto the grid of the simulation mesh and the initial self-consistent Poisson solution is obtained. In this case, the full Coulomb potential of the dopants

[a]Electronic mails: mgilbert@mer.utexas.edu and mgilbert@mail.utexas.edu

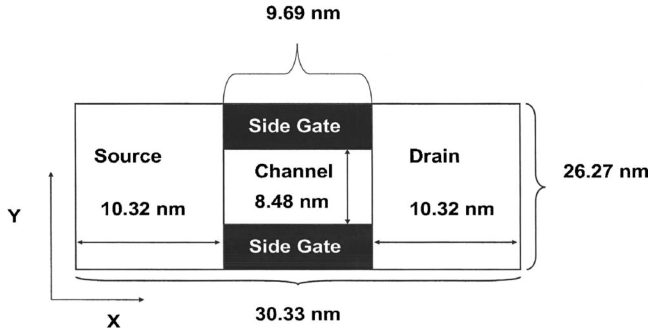

FIG. 1. Schematic of the trigate InAs quantum wire MOSFET in the xy plane.

is incorporated. Then, the solution of Poisson's equation for the local potential is no longer smoothly varying in the source and the drain of the device. The inclusion of discrete dopants causes the formation of potential variation in the source and drain. The density throughout the device is calculated using a variant of the recursive scattering matrix method which solves the Schrödinger equation in the effective mass approximation as described in Ref. 2. In short, this method provides us with a three-dimensional, fully quantum mechanical method. Since the transport calculation is performed in real space, the different excited modes in the system are automatically coupled unlike in other simulations.[3] In order to achieve self-consistency, the density obtained from the transport calculation is then updated using Broyden's method[10] and a new guess for the potential is obtained through the solution of Poisson's equation. The process is repeated until a desired level of convergence is obtained. Exchange and correlation terms are included through a local density approximation.[11] All of the simulations are performed at 300 K and a static drain current of V_d=0.6 V is applied.

III. POLAR OPTICAL PHONON SCATTERING

The inclusion of separable scattering mechanisms is not a new concept. In previous work, acoustic and optical phonon processes have been derived[4] and so the work will not be repeated here. However, we are now interested in including polar optical phonons which, to this point, have not been treated. We begin by noting that to use the method presented in Ref. 4, we are assuming that the scattering is weak relative to the energies in the system and that we are only interested in the steady state limit. Therefore, we can use the Fermi golden rule expression, equivalent to a first-order, non-self-consistent Born approximation, for each of the scattering processes and generate a real-space self-energy from it. In particular, we note that the imaginary part of the self-energy term is related to the scattering rate and it is the latter scattering rate that we wish to calculate.[4] This will result in an x directed momentum which is related to the carrier energy in the quantum wire. Since many of the details of the derivation of similar scattering rates are outlined in Ref. 4, we will show only the important changes in the derivation. In this article, we use the Fermi golden rule for scattering. This is treated in many other places and the only modification that we need is to account for the transverse modes of the quantum wire. Therefore, we begin with the general form

$$\left(\frac{1}{\tau_{\text{polar}}}\right)_{nm}^{n'm'} = \frac{\pi e^2}{\gamma V \omega_0}\sum_{q_x}\sum_{q_y,q_z}\int dy\int dz\int dy'\int dz'\,\varphi_{i,j}^{*}\times(y,z)\varphi_{i',j'}(y,z)\varphi_{i,j}^{*}(y',z')\varphi_{i',j'}(y',z')\times\frac{e^{iq_y(y-y')+iq_z(z-z')}}{q^2}\{(N_q+1)\delta(E_k-E_{k-q}-\hbar\omega_0)+N_q\delta(E_k-E_{k-q}+\hbar\omega_0)\}. \quad (1)$$

The delta functions in Eq. (1) serve to conserve the energy in the process of the interactions of the carriers with the polar optical phonons. $\varphi_{i,j}(y,z)$ is the transverse two-dimensional wave function in the particular slice under consideration. In Eq. (1), γ is the effective interaction parameter, ω_0 is the phonon frequency, V is the volume, mn are the initial subband indices, $m'n'$ are the final subband indices, q_x, q_y, and q_z are the phonon wave numbers in the x, y, and z directions, N_q is the Bose-Einstein distribution function for phonons, E_k is the current subband energy, and E_{k-q} is the final subband phonon energy after scattering. We assume in this treatment that we are dealing with parabolic band structure. Taking a closer look at the terms contained within the delta functions, we realize that based on this assumption

$$E_k - E_{k\pm q} \pm \hbar\omega_0 = E_{i,j} - E_{i',j'} \pm \hbar\omega_0 + \frac{\hbar^2 k_x^2}{2m_x^*} - \frac{\hbar^2(k_x \pm q_x)^2}{2m_x^*} = E_{i,j} - E_{i',j'} \pm \hbar\omega_0 \mp \frac{\hbar^2 k_x q_x}{m_x^*} - \frac{\hbar^2 q_x^2}{2m_x^*}. \quad (2)$$

In Eq. (2), E_{ij} and $E_{i'j'}$ are the initial and final energies at the bottom of their respective bands. We begin to simplify Eq. (1) by first examining the longitudinal terms

$$\sum_{q_z}\frac{1}{2q^2}\delta(E_k - E_{k\pm q} \pm \hbar\omega_0). \quad (3)$$

We now expand Eq. (3) using the results from Eq. (2),

$$\sum_{q_z}\frac{1}{q_x^2+q_y^2+q_z^2}\delta\left(\mp\frac{\hbar^2 q_x^2}{2m_x^*} \mp \frac{\hbar^2 k_x q_x}{m} + E_{i,j} - E_{i',j'} \pm \hbar\omega_0\right). \quad (4)$$

This sum may be simplified further by taking the Fourier transform,

$$\frac{1}{2\pi}\int_{-\infty}^{\infty}\frac{e^{iq_x(x-x')}}{q_x^2+q_y^2+q_z^2}\delta\left(\mp\frac{\hbar^2 q_x^2}{2m_x^*} \mp \frac{\hbar^2 k_x q_x}{m} + \Delta_{i,j}^{i',j'}\right)dq_x, \quad (5)$$

where

$$\Delta_{i,j}^{i',j'} = E_{i,j} - E_{i',j'} \pm \hbar\omega_0. \quad (6)$$

Representing Eq. (5) as a summation, we have

$$\frac{1}{2\pi}\sum_i \frac{e^{iq_x(x-x')}}{q_{xi}^2+q_y^2+q_z^2}\frac{1}{|\partial E_{k\pm q}/\partial q_x|} = \frac{m_x^*}{2\pi\hbar^2}\sum_i \frac{e^{iq_x(x-x')}}{q_{xi}^2+q_y^2+q_z^2}\frac{1}{|\mp k_x+q_{xi}|}. \quad (7)$$

At this point we examine the relationship for $E_{k\pm q}$,

$$E_{k\pm q} = \frac{\hbar^2 k_x^2}{2m_x^*} \pm \frac{\hbar^2 k_x q_x}{m_x^*} + \frac{\hbar^2 q_x^2}{2m_x^*}. \quad (8)$$

Equation (8) is quadratic in q_x and may then be solved to yield a solution for q_x which is then substituted back into Eq. (7) making the term in the absolute value independent of q_x as shown below regardless if the phonon process under consideration is emission or absorption. Therefore, we may group all of the variables that are independent of q_x into a simple dummy variable a. With this pairing, we may reduce our summation in Eq. (7) to reach

$$\frac{m_x^*}{2\pi\hbar^2}\sum_i \frac{e^{iq_x(x-x')}}{q_{xi}^2+a^2}. \quad (9)$$

Equation (9) is most easily evaluated by making a transformation to cylindrical coordinates to obtain

$$\frac{m_x^*}{4\pi^2\hbar^2}\int\int \frac{q_x e^{iq_x(\mathbf{r_x}-\mathbf{r_x'})}}{q_x^2+a^2}d\theta dq. \quad (10)$$

We evaluate the integral in Eq. (10) using contour integrations to arrive at a final, simplified expression for the sum over the longitudinal wave vectors

$$\sum_{q_x}\frac{1}{2q_x}\delta(E_k). \quad (11)$$

The expression in Eq. (11) is substituted back into Eq. (1) to find an overlap integral that is similar to both the one found in Ref. 9 and in most textbooks,

$$= \sum_{q_x}\sum_{q_y,q_z}\int dy\int dz\int dy'\int dz'\,\varphi_{i,j}^*(y,z)\varphi_{i',j'}(y,z)\varphi_{i,j}^*(y',z')\varphi_{i',j'}(y',z') \times \frac{e^{iq_y(y-y')+iq_z(z-z')}}{2q_x}\delta(E_k) = \frac{A}{2V}\sum_{q_x} \times\int\int dzdy[\varphi_{i,j}^*(y,z)\varphi_{i',j'}(y,z)]^2\frac{1}{q_x}\delta(E_k) = \frac{A}{4\pi V}\sum_{k_x} I_{i,j}^{i',j'}\frac{1}{k_x}\delta(E_k), \quad (12)$$

where in Eq. (12) we have used the following definition:

$$I_{i,j}^{i',j'} = \frac{A}{4\pi^2 V}\int\int dydz[\varphi_{i,j}^*(y,z)\varphi_{i',j'}(y,z)]^2. \quad (13)$$

Following the usual procedure, we replace the summation over the final momentum states with an integration

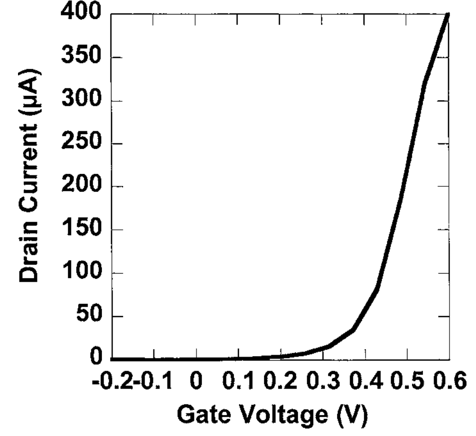

FIG. 2. I_d-V_g curve with only elastic scattering processes included.

$$\sum_{k'} \to \frac{L}{2\pi}\int_{-\infty}^{\infty} dk' = \int_0^{\infty}\rho_{1D}(E')dE' \quad (14)$$

to obtain the final result

$$\left(\frac{1}{\tau_{\text{polar}}}\right)_{i,j}^{i',j'} = \frac{m_x^* L e^2}{32\pi^3\gamma\omega_0} I_{i,j}^{i',j'}\int\frac{dk_x}{k_x}\delta(E_k). \quad (15)$$

However, we are still in the mode space representation and the longitudinal momentum is not yet a viable operator. To remedy this, we take the inverse transform. This essentially involves solving a contour integral for both the emission and absorption cases which results from Eq. (15). This gives us our final, simplified and summarized results for absorption and emission of POPs,

$$\left(\frac{1}{\tau_{\text{polar}}}\right)_{i,j}^{i',j'} = \frac{m_x^* L e^2}{32\pi^3\gamma\omega_0} I_{i,j}^{i',j'}\begin{cases} N_q e^{-k_0|x-x'|} \\ (N_q+1)\dfrac{\sin(k_0|x-x'|)}{k_0|x-x'|} \end{cases}. \quad (16)$$

In Eq. (16), k_0 is the phonon wave number. This is a rather expected result as we now see the manifestation of the nonlocal nature of POP scattering as we see a clear dependence on the grid in Eq. (16). To utilize this in the transport calculation, we must use the following unitary transformation to convert this form to the site representation for inclusion in the Hamiltonian:

$$\Gamma_{\text{polar}} = \text{Im}\{\Sigma\} = U^{+}\left(\frac{\hbar}{\tau_{\text{polar}}}\right)_{i,j}^{i',j'} U, \quad (17)$$

where U is a unitary mode-to-site transformation matrix. The unitary matrix U^{+} results from the eigenvalue solutions in the transverse slice and are composed of the various eigenfunctions in the site basis. Hence, it represents a mode-to-slice transformation.

IV. RESULTS AND DISCUSSION

In Fig. 2, we plot the I_d-V_g curve for a discretely doped trigate InAs quantum wire devices with only elastic scatter-

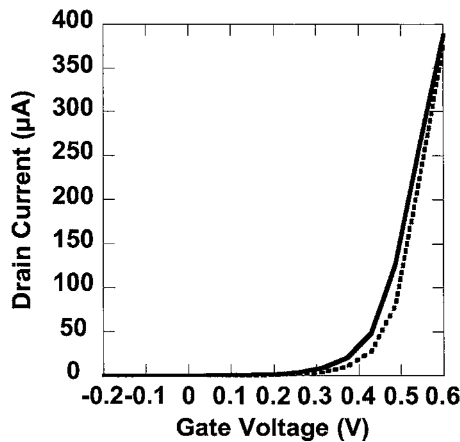

FIG. 3. I_d-V_g curves for elastic scattering processes (solid) and a combination of elastic and inelastic scattering (dotted) included.

ing considered. Speaking in terms of simple device performance, averaging over four different devices, we find that the threshold voltage is found to be 0.373 V±11 mV. These figures are slightly different from those quoted elsewhere,[12] but it should be noted that we have used a smaller sampling of devices in this study. While the threshold voltage is, at present, too high for next generation technology, with the use of gate stack engineering,[12] this figure can be brought down to acceptable levels. Furthermore, we see that the spread in the threshold voltage is quite small. This is due to the fact that fewer dopant atoms are required to reach these levels of performance. Thus, with fewer elastic scattering sights to induce quantum interference, the threshold voltage is expected to be more stable than in its silicon based equivalents.

In Fig. 3, we utilize the same dopant distribution as in Fig. 2 and now include the phonon processes in addition to the electron-impurity interactions. Due to the fact that in InAs the X and L valleys are offset from the Γ valley by large energy offsets, the contribution of intervalley scattering will typically be quite small for the voltages applied to the device here. By limiting the effectiveness of the intervalley processes and with the already small acoustic deformation potential scattering, we find a situation where basically the only inelastic process is that of POP scattering. Examining the curves, we find that in the low gate voltage regime POP scattering significantly reduces the current. This shift in low gate voltage current leads to modifications to the performance. The threshold voltage averaged over four devices is 0.423 V±7 mV. Based on this result, we find that the POP scattering does indeed shift the threshold voltage, but it also stabilizes this device measure by reducing spread in carrier energy in the source.

At high gate voltages, we find that the current in both the elastic and combined (elastic scattering contribution +inelastic scattering contribution) cases that the drain currents begin to merge after $V_g=0.5$ V. This can be most directly attributed to a high energy localization of the POP scattering rate. This localization reduces the scattering rate as less of the nonlocal contribution influences the rate. Therefore, the inelastic perturbations to the current tend to become negligible and we are left only with the elastic interactions.

We seek to confirm this result by examining the electron densities for the elastic and combined cases. In Fig. 4, we plot the electron densities taken at depths of approximately 5 nm into the InAs device layer. The black dots in the figure represent the locations of the dopant atoms in the system. Dots that are larger in size are closer to the surface of the device, while dots that are smaller are buried farther down in the device. In Fig. 4(a) we plot the density at $V_g=0.6$ V for the elastic case. At this voltage, we are clearly above the threshold voltage for the device. The channel is now fully populated with carriers. In the source and drain, the location of the electron density depends rather weakly on the locations of the dopants. This is mainly due to the scarcity of the dopants and that they are buried deeply in the InAs substrate which reduces their effect on the propagating electrons. Nev-

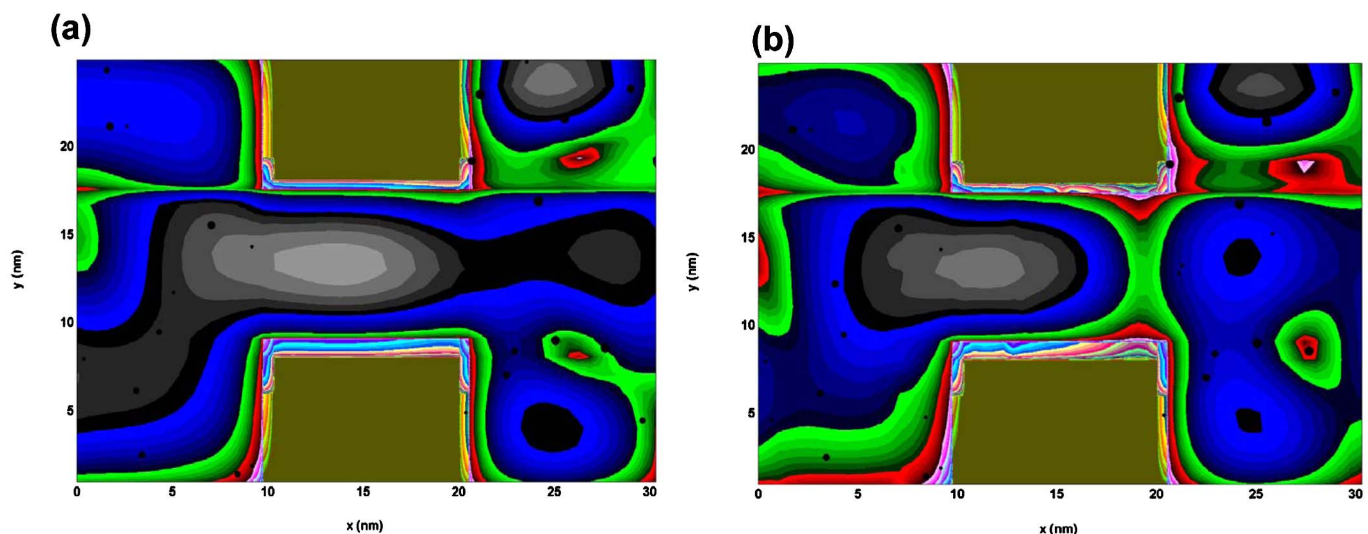

FIG. 4. Electron density in the xy plane taken at a depth of approximately 5 nm into the InAs device layer for (a) elastic and (b) combined processes.

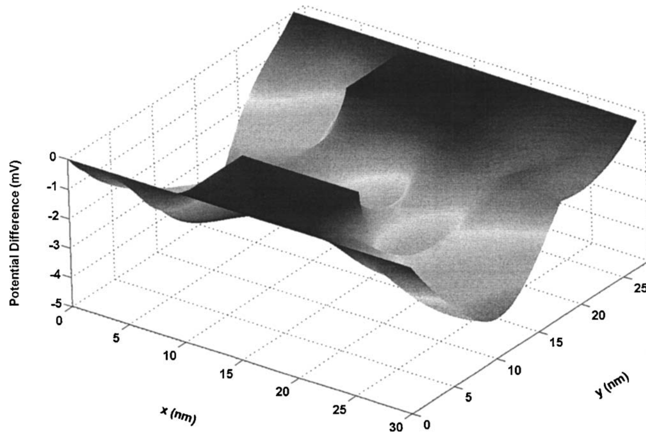

FIG. 5. Potential discrepancy between the combined processes and the elastic only processes taken at a depth of approximately 5 nm into the InAs layer.

ertheless, the density tends to roughly follow the path of the dopants as it makes its way to the channel. In the channel, we find that the some of the density has been trapped by multiple sequential reflections off the source-channel and channel-drain interfaces. As the density then exits the channel, it begins to populate sites in the drain that are energetically preferential.

In Fig. 4(b), we plot the density at $V_g=0.6$ V for the combined case. We see some distinct differences in the location and magnitude of the electrons in the combined case, but, in general, it follows the same general trend as in the elastic case. With the combined case, we find that there is a more pronounced null near the drain end of the channel. The reflection off this interface alters the energy of the carriers to the point where some of the lower energy modes will see increased scattering and a reduction in density. In the source, we find additional discrepancies as this is the location where the scattering is most prevalent. Here we find large reflections due to the scattering in low energy modes, but as the density approaches the channel and gains energy, the discrepancies become much smaller due to the reduction in scattering. In Fig. 5, we provide further confirmation in the form of a plot of the difference between the potentials resulting from the elastic and combined cases at $V_g=0.6$ V. This plot confirms much of what we previously stated. We find a large discrepancy in potential, and therefore density, in the source corresponding to large scattering rates. As we progress through the device, we find that the differences are markedly smaller as the scattering rate is reduced. Only in the areas where reflections off the interfaces play a role do we see any appreciable differences, but these interactions are small enough to cause no significant effect to the overall drain current.

V. CONCLUSIONS

We have presented results of three-dimensional, self-consistent quantum device simulations. We find that in devices with deeply buried dopant atoms the inclusion of inelastic processes has a non-negligible effect on the device performance at low gate voltages leading to shifts in the threshold voltage. This result is due mainly to the POP scattering effect as the quantum interference generated by the discrete dopants is minimized due to their location away from the charge centroid. At higher gate voltages, we find that the POP scattering switches from an inherently nonlocal process to a local one. This led to decreased inelastic interactions which allowed the device to recover ballistic performance. The recovery of ballistic performance at room temperature gives rise to the possibility of fabricating devices with lengths less than the phonon scattering lengths for ultrahigh performance.

ACKNOWLEDGMENT

This work is supported by NRI, AMRC, SRC, ONR, and Intel Corporation.

[1]H. S. Doyle, S. Datta, M. Doczy, S. Hareland, B. Jin, J. Kavalieros, T. Linton, A. Murthy, R. Rios, and R. Chau, IEEE Electron Device Lett. **24**, 263 (2003).
[2]M. J. Gilbert and D. K. Ferry, J. Appl. Phys. **95**, 7954 (2004).
[3]J. Wang, E. Polizzi, and M. Lundstrom, J. Appl. Phys. **96**, 2192 (2004).
[4]M. J. Gilbert, R. Akis, and D. K. Ferry, J. Appl. Phys. **98**, 094303 (2005).
[5]J. B. Boos, W. Krupps, D. Park, B. Molnar, and B. R. Bennett, Electron. Lett. **32**, 688 (1996).
[6]C. R. Bolognesi, E. J. Caine, and H. Kroemer, IEEE Electron Device Lett. **15**, 16 (1994).
[7]R. Chau, S. Datta, M. Doczy, B. Doyle, B. Jin, J. Kavalieros, A. Majumdar, M. Metz, and M. Radosavljevic, IEEE Trans. Nanotechnol. **4**, 153 (2005).
[8]S. Jin, Y. J. Park, and H. S. Min, J. Appl. Phys. **99**, 123719 (2006).
[9]M. J. Gilbert and D. K. Ferry, Superlattices Microstruct. **34**, 277 (2003).
[10]D. D. Johnson, Phys. Rev. B **38**, 12807 (1988).
[11]Y. Wang, J. Wang, H. Guo, and E. Zaremba, Phys. Rev. B **52**, 2738 (1995).
[12]M. J. Gilbert and D. K. Ferry, J. Appl. Phys. **99**, 054503 (2006).